CHAPTER

Incompressible Non-Newtonian Flows

5

5.1 Introduction

In this chapter we discuss briefly the non-Newtonian effect in flow problems. In non-Newtonian flow cases, the viscosity of the material is nonlinearly dependent on the stress or strain rate and their magnitudes. There are several models available for non-Newtonian fluids. The simplest and widely used among these models is the one based on the *power law*. We start with such a formulation for metal and polymer forming in Section 5.2. Fluids that partially return to the original form when applied stress is released are called *viscoelastic*. The models for viscoelastic fluids can be quite complicated. In Section 5.3 we provide such models and discuss their numerical solution using the CBS procedure described in Chapter 3. In Section 5.4 we briefly discuss a direct displacement method based on the CBS approach to impact problems.

5.2 Non-Newtonian flows: Metal and polymer forming

5.2.1 Non-Newtonian flows including viscoplasticity and plasticity

In many fluids the viscosity, though isotropic, may be dependent on the rate of strain $\dot{\varepsilon}_{ij}$ as well as on the state variables such as temperature or total deformation. Typical here is, for instance, the behavior of many polymers, hot metals, blood in small arteries, etc., where a power law of the type

$$\mu = \mu_0 \dot{\bar{\varepsilon}}^{(m-1)} \tag{5.1}$$

with

$$\mu_0 = \mu_0(T, \bar{\varepsilon})$$

governs the viscosity-strain rate dependence where m is a physical constant. In the above $\dot{\bar{\varepsilon}}$ is the second invariant of the deviatoric strain rate tensor defined from Eq. (3.36), T is the (absolute) temperature, and $\bar{\varepsilon}$ is the total strain invariant.

This *secant* viscosity can of course be obtained by plotting the relation between the deviatoric stresses and deviatoric strains or their invariants, as Eq. (3.35) simply defines the viscosity by the appropriate ratio of the stress to strain rate. Such plots are shown in Fig. 5.1 where $\bar{\sigma}$ denotes the second deviatoric stress invariant. The above power law relation of Eq. (5.1) is known as the Oswald de Wahle law (or power law) and is illustrated in Fig. 5.1b.

Finite Element Meth Fluid Dynam 7E, Volume 3. http://dx.doi.org/10.1016/B978-1-85617-635-4.00005-4

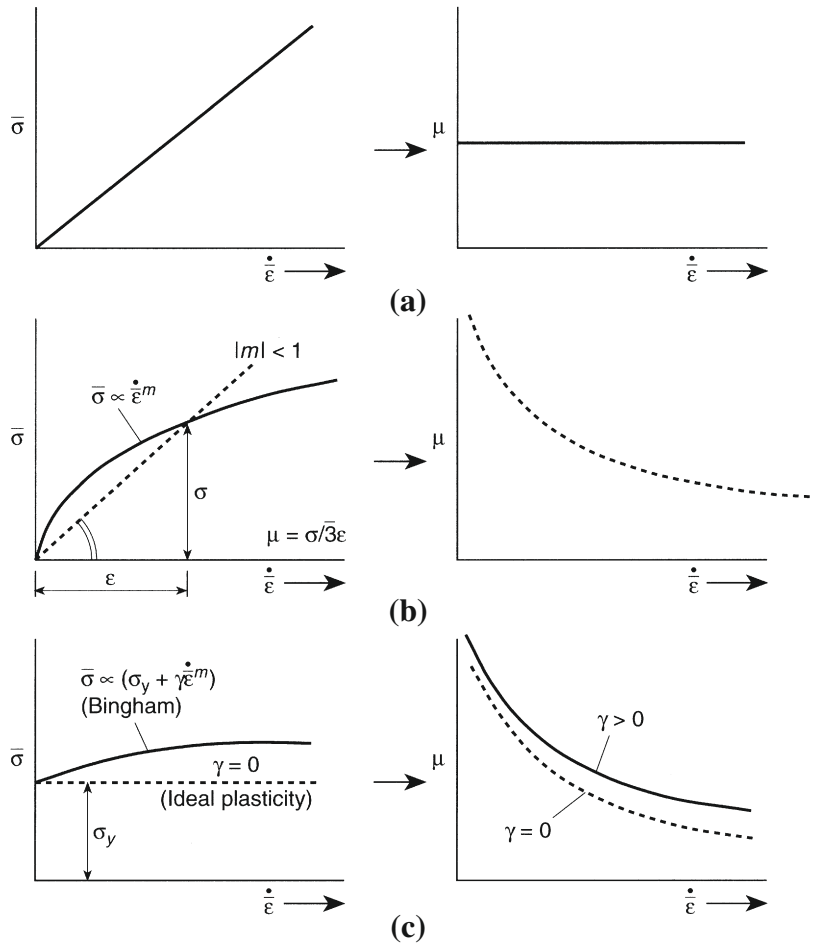

FIGURE 5.1

Stress $\bar{\sigma}$, viscosity μ, and strain rate $\dot{\bar{\varepsilon}}$ relationships for various materials: (a) linear, Newtonian, fluid; (b) non-Newtonian polymers; (c) viscoplastic-plastic metals.

In a similar manner viscosity laws can be found for viscoplastic and indeed purely plastic behavior of an incompressible kind. For instance, in Fig. 5.1c we show a viscoplastic Bingham fluid in which a threshold or yield value of the second stress invariant has to be exceeded before any strain rate is observed. Thus for the viscoplastic fluid illustrated it is evident that a highly nonlinear viscosity relation is obtained. This can be written as

$$\mu = \frac{\bar{\sigma}_y + \gamma \dot{\bar{\varepsilon}}^m}{\dot{\bar{\varepsilon}}} \tag{5.2}$$

where $\bar{\sigma}_y$ is the value of the second stress invariant at yield.

The special case of pure plasticity follows of course as a limiting case when the fluidity parameter $\gamma = 0$, and now we have simply

$$\mu = \frac{\bar{\sigma}_y}{\dot{\bar{\varepsilon}}} \tag{5.3}$$

Of course, once again $\bar{\sigma}_y$ can be dependent on the *state* of the fluid, i.e.,

$$\bar{\sigma}_y = \bar{\sigma}_y(T, \bar{\varepsilon}) \tag{5.4}$$

The solutions (at a given state of the fluid) can be obtained by various iterative procedures, noting that Eq. (4.31) continues to be valid but now with the matrix $\mathbf{K}$ being dependent on viscosity, i.e.,

$$\mathbf{K} = \mathbf{K}(\mu) = \mathbf{K}(\dot{\bar{\varepsilon}}) = \mathbf{K}(\mathbf{u}) \tag{5.5}$$

thus being dependent on the solution.

The total iteration process can be used simply here (see Ref. [1]). Thus rewriting Eq. (4.31) as

$$\mathbf{A} \begin{Bmatrix} \tilde{\mathbf{u}} \\ \tilde{\mathbf{p}} \end{Bmatrix} = \begin{Bmatrix} \bar{\mathbf{f}} \\ \mathbf{0} \end{Bmatrix} \tag{5.6}$$

and noting that

$$\mathbf{A} = \mathbf{A}(\tilde{\mathbf{u}}, \tilde{\mathbf{p}})$$

we can write

$$\begin{Bmatrix} \tilde{\mathbf{u}} \\ \tilde{\mathbf{p}} \end{Bmatrix}^{n+1} = \mathbf{A}_n^{-1} \begin{Bmatrix} \bar{\mathbf{f}} \\ \mathbf{0} \end{Bmatrix} \qquad \mathbf{A}_n = \mathbf{A}(\tilde{\mathbf{u}}, \tilde{\mathbf{p}})^n \tag{5.7}$$

Starting with an arbitrary value of μ we repeat the solution until convergence is obtained.

Such an iterative process converges rapidly (even when, as in pure plasticity, μ can vary from zero to infinity), providing that the forcing $\bar{\mathbf{f}}$ is due to *prescribed boundary velocities* and thus immediately confines the variation of all velocities in a narrow range. In such cases, five to seven iterations are generally required to bring the difference of the nth and $(n + 1)$th solutions to within the 1% (Euclidian) norm.

The first non-Newtonian flow solutions were applied to polymers and to hot metals in the early 1970s [2,3]. Application of the same procedures to the forming of metals was introduced at the same time and has subsequently been widely developed [4–33].

It is perhaps difficult to visualize steel or aluminum behaving as a fluid, being conditioned to use these materials as structural members. If, however, we note that during the forming process the elastic strains are of the order of 10^{-6} while the plastic strain can reach or exceed a value of unity, neglect of the former (which is implied in the viscosity definition) seems justifiable. This is indeed born out by comparison of computations based on what we now call *flow formulation* with elastoplastic computation or experiment. The process has alternatively been introduced as a "rigid-plastic" form [12,14], though such modeling is more complex and less descriptive.

Today the methodology is widely accepted for the solution of metal and polymer forming processes, and only a limited selection of references of application can be

cited. The reader would do well to consult Refs. [20,34–38] for a complete survey of the field.

5.2.2 Steady-state problems of forming

Two categories of problems arise in forming situations. *Steady-state flow* is the first of these. In this, a real, continuing, flow is modeled, as shown in Fig. 5.2a and here velocity and other properties can be assumed to be fixed in a particular point of space. In Fig. 5.2b the more usual *transient* processes of forming are illustrated and we shall deal with these later. In a typical steady-state problem if the state parameters T and $\bar{\varepsilon}$ defining the temperature and total strain invariant are known in the whole field, the solution can be carried out in the manner previously described. We could, for instance, assume that the "viscous" flow of the problem of Fig. 5.3 is that of an ideally plastic material under isothermal conditions modeling an extrusion process and obtain the solution shown in Table 5.1. For such a material exact extrusion forces can be calculated [39] and the table shows the errors obtained with the flow formulation using the different triangular elements of Fig. 5.3 and two meshes [40]. The fine mesh here was arrived at by using error estimates and a single adaptive remeshing.

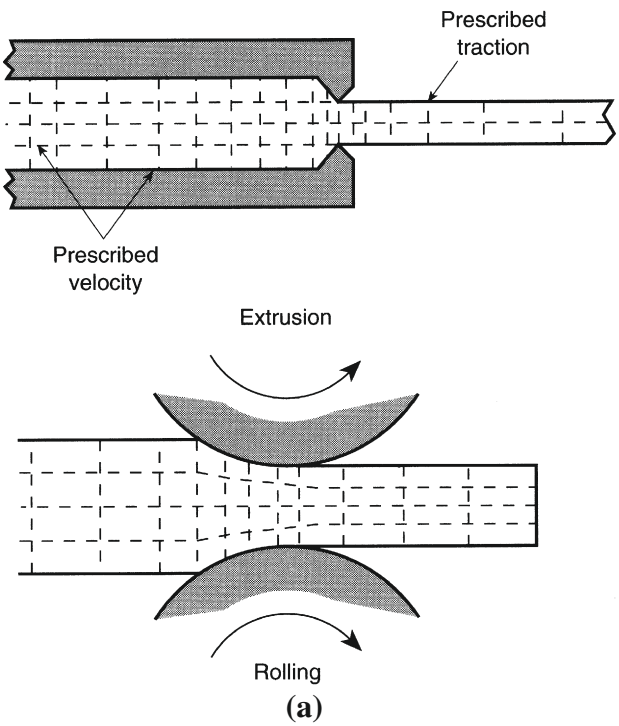

FIGURE 5.2
Forming processes typically used in manufacture: (a) steady rate; (b) transient.

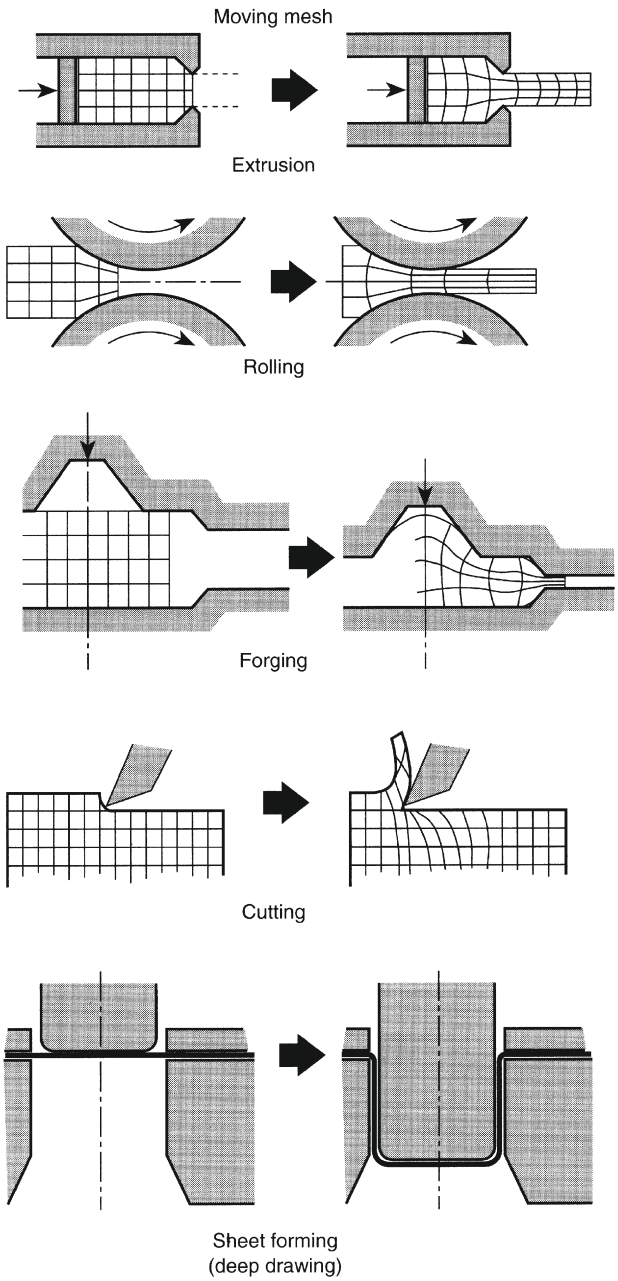

FIGURE 5.2
(*Continued*).

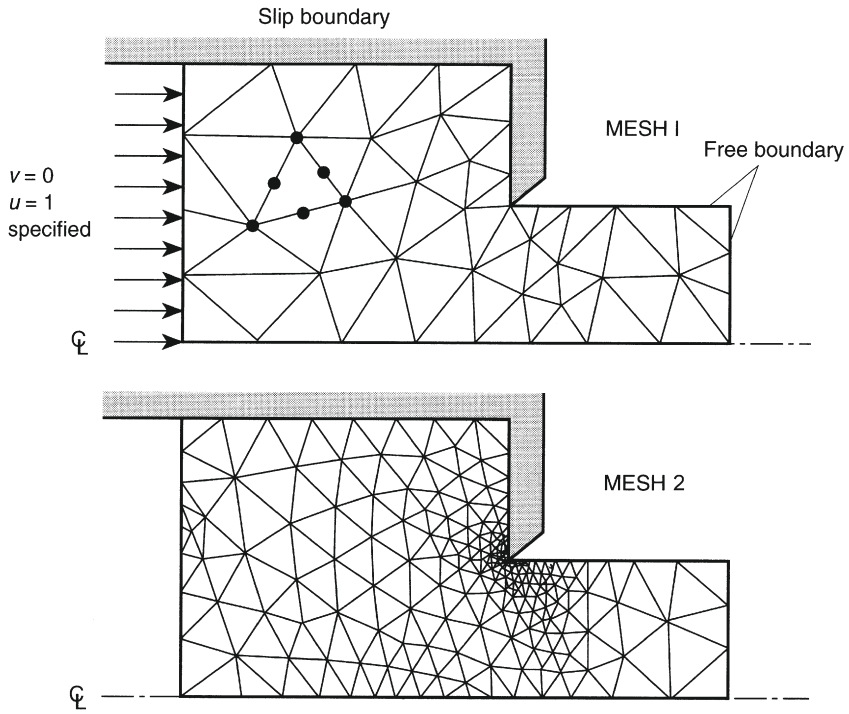

FIGURE 5.3
Plane strain extrusion (extrusion ratio 2:1) with ideal plasticity assumed.

Table 5.1 Comparisons of Performance of Several Triangular Mixed Elements of Fig. 5.3 in a Plane Extrusion Problem (ideal plasticity assumed) [40]

	Mesh 1 (coarse)			Mesh 2 (fine)		
Element Type	**Ext. Force**	**Force Error**	**CPU(s)**	**Ext. Force**	**Force Error**	**CPU(s)**
T6/1D	28,901.0	12.02	67.81	25,990.0	0.73	579.71
T6B1/3D	31,043.0	20.32	75.76	26,258.0	1.78	780.13
T6B1/3D*	29,031.0	12.52	73.08	26,229.0	1.66	613.92
T6/3C	27,902.5	8.15	87.62	25,975.0	0.67	855.38
Exact	25,800.0	0.00	–	25,800.0	0.00	–

In general the problem of steady-state flow is accompanied by the evolution of temperature (and other state parameters such as the total strain invariant $\bar{\varepsilon}$) and here it is necessary to couple the solution with the heat balance and possibly other evolution equations. The evolution of heat has already been discussed and the appropriate conservation equations such as Eq. (4.6) can be used. It is convenient now to rewrite this equation in a modified form.

Firstly, we note that the kinetic energy is generally negligible in the problems considered and that with a constant heat capacity $\hat{c}$ per unit volume we can write

$$\rho E \approx \rho e = \hat{c}T \tag{5.8a}$$

Secondly, we observe that the internal work dissipation can be rewritten by the identity

$$\frac{\partial}{\partial x_i}(pu_i) - \frac{\partial}{\partial x_j}(\tau_{ji}u_i) \equiv -\sigma_{ji}\dot{\varepsilon}_{ji} \tag{5.8b}$$

where, by Eq. (1.9a),

$$\sigma_{ji} = \tau_{ji} - \delta_{ji}p \tag{5.8c}$$

and, by Eq. (1.2),

$$\dot{\varepsilon}_{ji} = \frac{1}{2}\left(\frac{\partial u_j}{\partial x_i} + \frac{\partial u_i}{\partial x_j}\right) \tag{5.8d}$$

We note in passing that in general the effect of the pressure term in Eq. (5.8b) is negligible and can be omitted if desired.

Using the above and inserting the incompressibility relation we can write the energy conservation as [for an alternative form see Eq. (4.6)]

$$\left(\hat{c}\frac{\partial T}{\partial t} + \hat{c}u_i\frac{\partial T}{\partial x_i}\right) - \frac{\partial}{\partial x_i}\left(k\frac{\partial T}{\partial x_i}\right) - (\sigma_{ij}\dot{\varepsilon}_{ij} + \rho g_i u_i) = 0 \tag{5.9}$$

The solution of the coupled problem can be carried out iteratively. Here the term in the last bracket can be evaluated repeatedly from the known velocities and stresses from the flow solution. We note that the first bracketed term represents a total derivative of the convective kind which, even in the steady state, requires the use of the special weighting procedures discussed in Chapter 2.

Such coupled solutions were carried out for the first time as early as 1973 and later in 1978 [7, 13], but are today practiced routinely.

Example 5.1. Steady-state rolling problem

Figure 5.4 shows a typical thermally coupled solution for a steady-state rolling problem from Ref. [13]. It is of interest to note that in this problem boundary friction plays an important role and that this is modeled by using thin elements near the boundary, making the viscosity coefficient in that layer pressure dependent [21]. This procedure is very simple and although not exact gives results of sufficient practical accuracy.

5.2.3 Transient problems with changing boundaries

These represent the second, probably larger, category of forming problems. Typical examples here are those of forging, indentation, etc., and again thermal coupling can be included if necessary. Figures 5.5 and 5.6 illustrate typical applications.

The solution for velocities and internal stresses can be readily accomplished at a given configuration, provided the temperatures and other state variables are known at that instant. This allows the new configuration to be obtained both for the boundaries

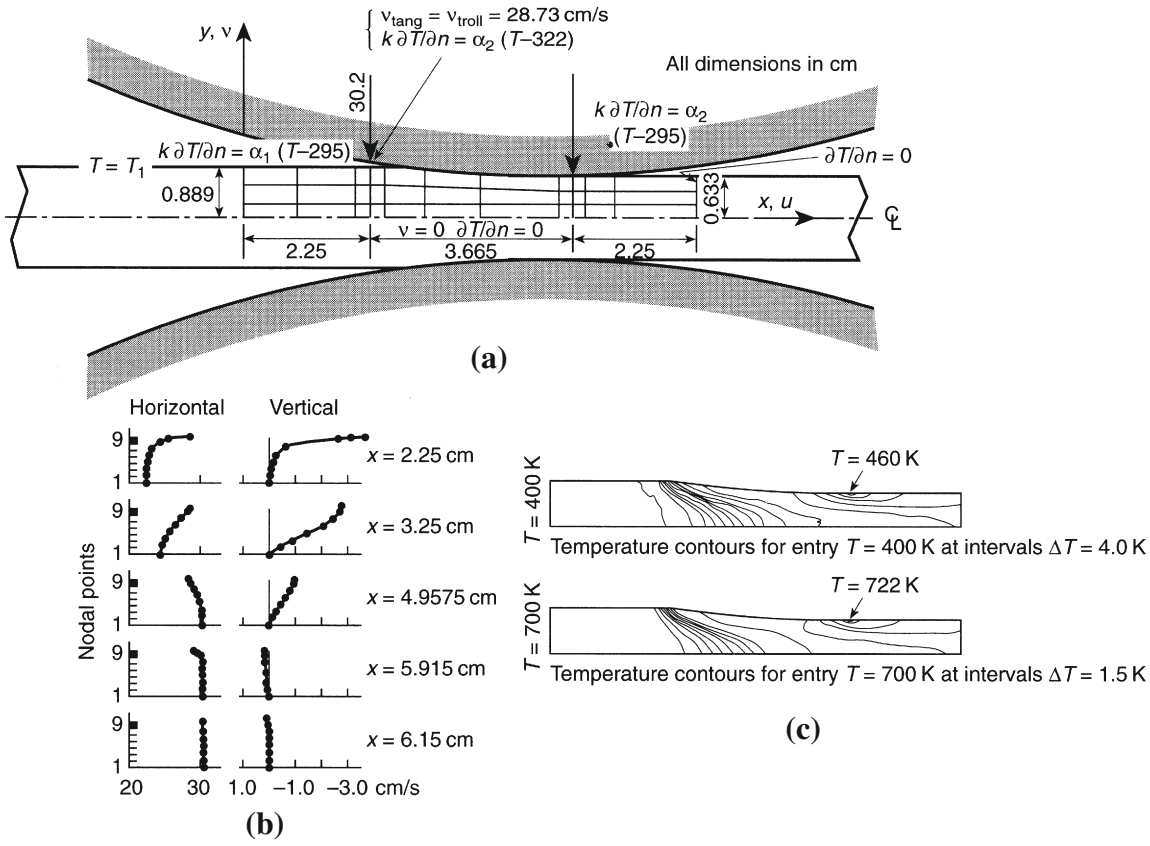

FIGURE 5.4

Steady-state rolling process with thermal coupling [40]: (a) geometry; (b) velocity profiles; (c) temperature distribution for different entry temperatures.

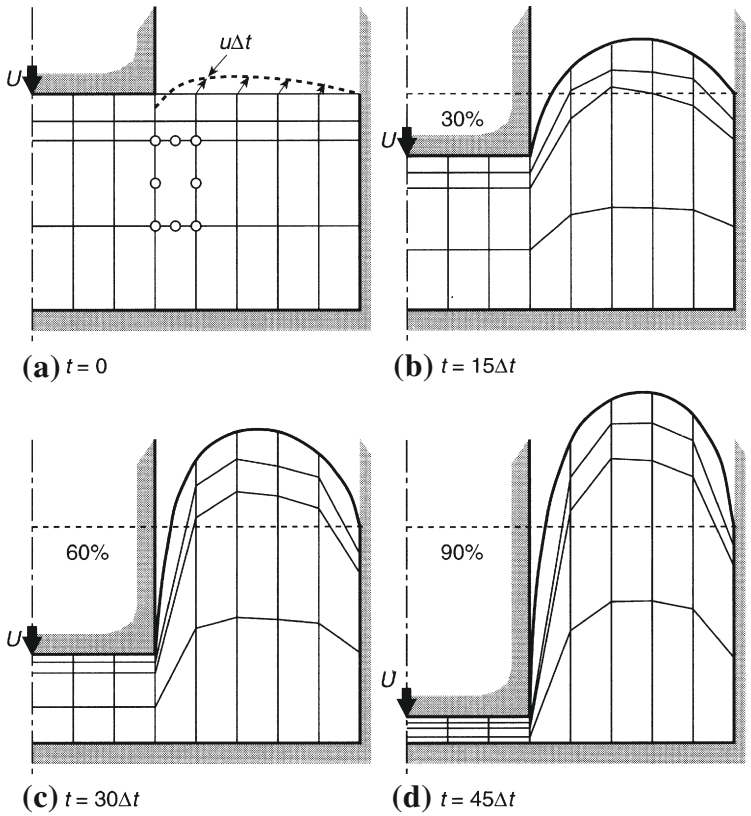

FIGURE 5.5

Punch indentation problem (penalty function approach) [4]. Updated mesh and surface profile with 24 isoparametric elements. Ideally plastic material; (a), (b), (c), and (d) show various depths of indentation (reduced integration is used here).

and for the mesh by writing explicitly

$$\Delta x_i = u_i \Delta t \tag{5.10}$$

as the incremental relation.

If thermal coupling is important increments of temperature need also to be evaluated. However, we note that for convected coordinates Eq. (5.9) is simplified as the convected terms disappear. We can now write

$$\hat{c}\frac{\partial T}{\partial t} - \frac{\partial}{\partial x_i}\left(k\frac{\partial T}{\partial x_i}\right) - (\sigma_{ij}\dot{\varepsilon}_{ij} + \rho g_i u_i + g_h) = 0 \tag{5.11}$$

where the last term is the heat input known at the start of the interval and computation of temperature increments is made using either explicit or implicit procedures discussed in Chapter 3.

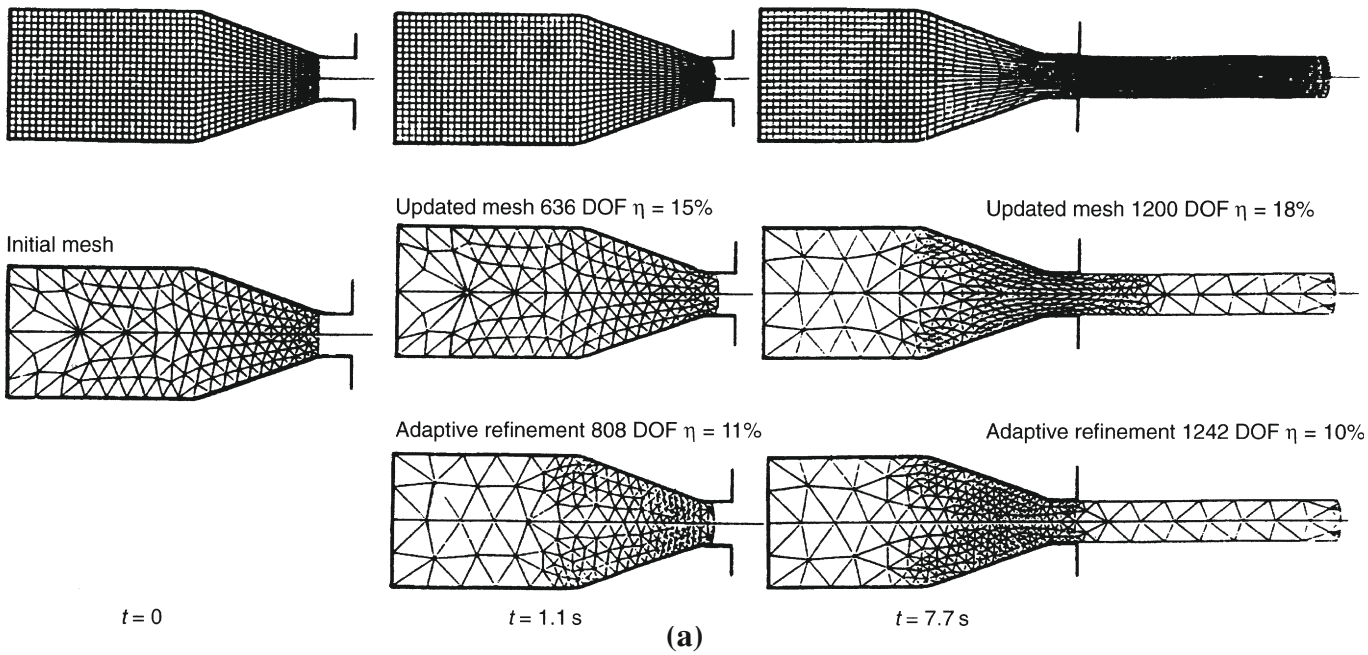

FIGURE 5.6

(a) A material grid and updated and adapted meshes with material deformation (η percentage in energy norm). A transient extrusion problem with temperature and strain-dependent yield [42]. Adaptive mesh refinement uses T6/1D elements of Fig. 4.20; (b) Contours of state parameters at $t = 2.9$ s; (c) load versus time.

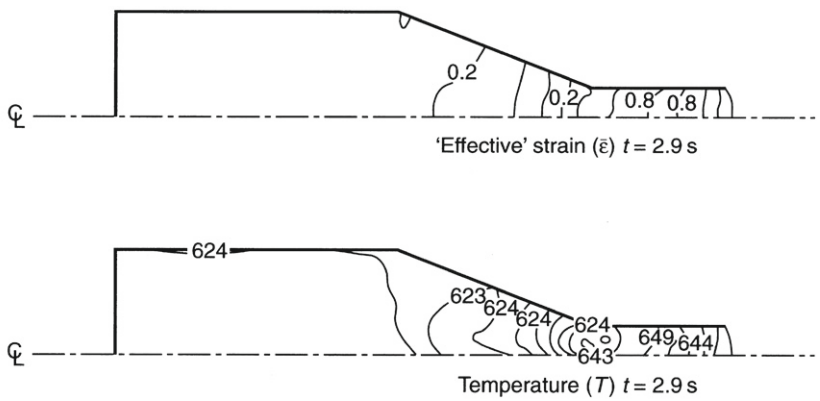

(b)

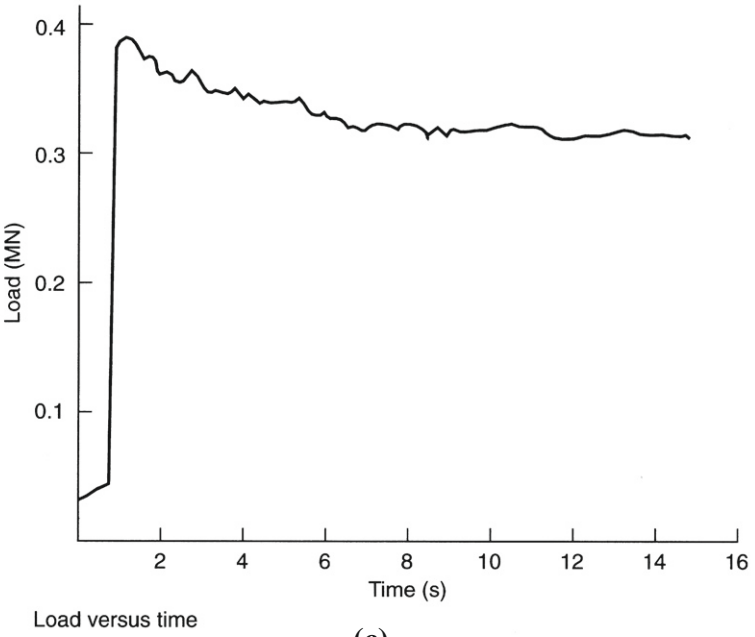

(c)

FIGURE 5.6
(*Continued*).

Indeed, both the coordinate and thermal updating can make use iteratively of the solution on the updated mesh to increase accuracy. However, it must be noted that any continuous mesh updating will soon lead to unacceptable meshes and some form of remeshing is necessary.

Example 5.2. Punch indentation problem

In the example of Fig. 5.5 [4], in which ideal plasticity was assumed together with isothermal behavior, it is necessary only to keep track of boundary movements. As temperature and other state variables do not enter the problem the remeshing can be done simply—in the case shown by keeping the same vertical lines for the mesh position.

Example 5.3. Transient extrusion problem

In the example of Fig. 5.6 showing a more realistic problem [41,42], when a new mesh is created an interpolation of all the state parameters from the old to the new mesh positions is necessary. In such problems it is worthwhile to strive to obtain discretization errors within specified bounds and to remesh adaptively when these errors are too large.

We have discussed the problem of adaptive remeshing for linear problems in Chapter 16 of Ref. [1]. In the present examples similar methods have been adopted with success [43,44] and in Fig. 5.6 we show how remeshing proceeds during the forming process. It is of interest simply to observe that here the *energy norm* of the error is the measure used.

The details of various applications can be found in the extensive literature on the subject. This also deals with various sophisticated mesh updating procedures. One particularly successful method is the so-called ALE (arbitrary Lagrangian-Eulerian) method [45–49]. Here the original mesh is given some prescribed velocity $\bar{\mathbf{v}}$ in a manner fitting the moving boundaries, and the convective terms in the equations are retained with reference to this velocity. In Eq. (5.9), for instance, in place of

$$\hat{c}u_i \frac{\partial T}{\partial x_i} \qquad \text{we write} \qquad \hat{c}(u_i - \bar{v}_i)\frac{\partial T}{\partial x_i}$$

etc., and the solution can proceed in a manner similar to that of steady state (with convection disappearing of course when $\bar{v}_i = u_i$, i.e., in the pure updating process). For more details on the ALE framework, readers are referred to Chapter 6.

It is of interest to observe that the flow methods can equally well be applied to the forming of thin sections resembling shells. Here of course all the assumptions of shell theory and corresponding finite element technology are applicable. Because of this, incompressibility constraints are no longer a problem but other complications arise. The literature of such applications is large, but much of the relevant information can be found in Refs. [50–62]. Practical applications ranging from the forming of beer cans to those of car bodies abound. Figures 5.7 and 5.8 illustrate some typical problems.

5.2.4 Elastic springback and viscoelastic fluids

In Section 5.2.1 we have argued that omission of elastic effects in problems of metal or plastic forming can be justified because of the small amount of elastic straining. This is undoubtedly true when we wish to consider the forces necessary to initiate large deformations and to follow these through. There are however a number of problems in which the inclusion of elasticity is important. One such problem is for instance that

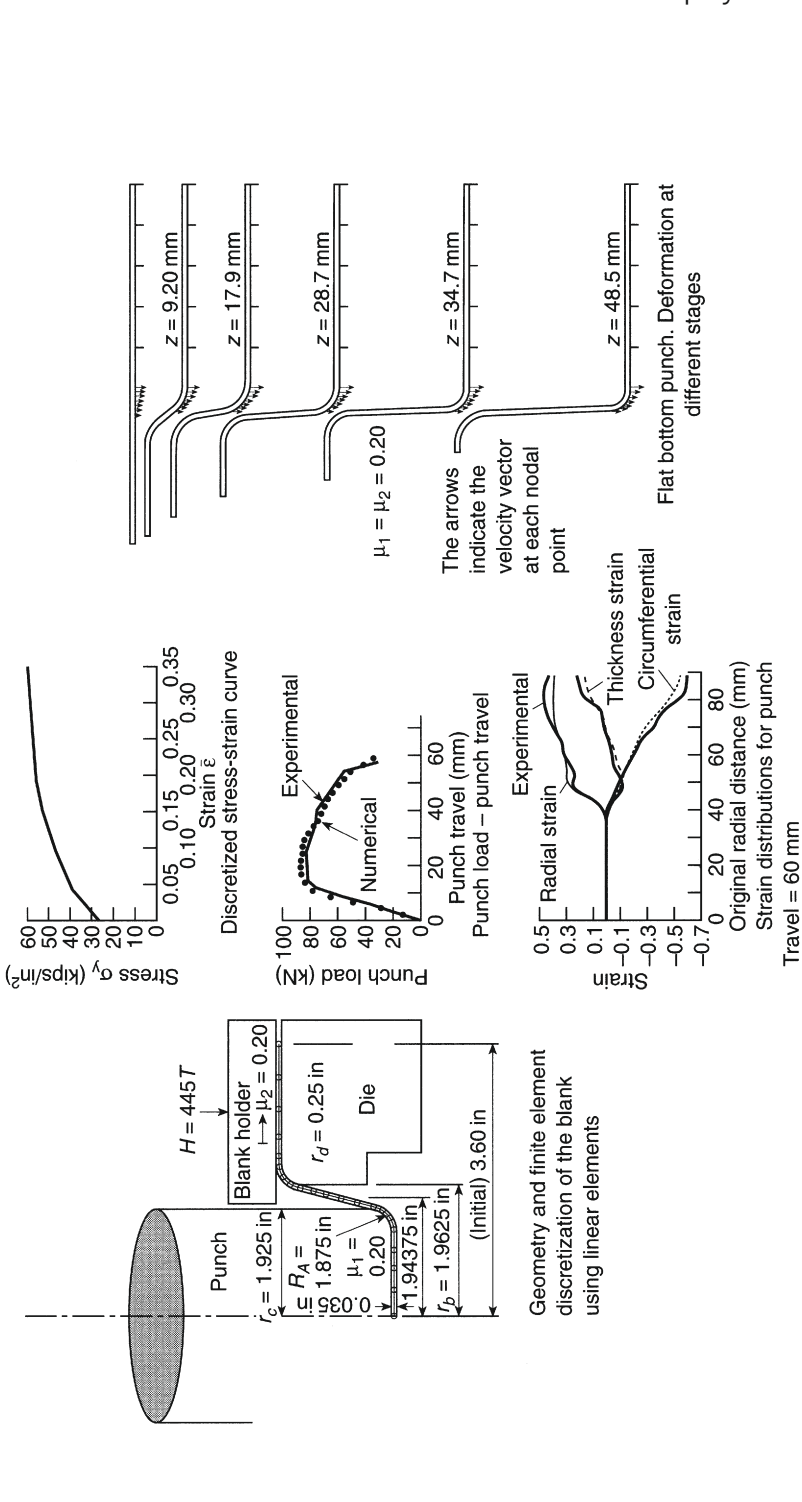

FIGURE 5.7
Deep drawing by a flat-nosed punch [50].

of "spring-back" occurring particularly in metal forming of complex shapes. Here it is important to determine the amount of elastic recovery which may occur after removing the forming loads. Some possible suggestions for the treatment of such effects have been presented in Ref. [21] as early as 1984. However since that time much attention has been focused on the flow of viscoelastic fluids, which is relevant to the above problem as well to the problem of transportation of fluids such as synthetic rubbers, etc. The procedures used in the study of such problems are quite complex and belong to the subject of numerical rheology [63–86]. Obviously the subject is vast and here we shall give a brief summary of the topic.

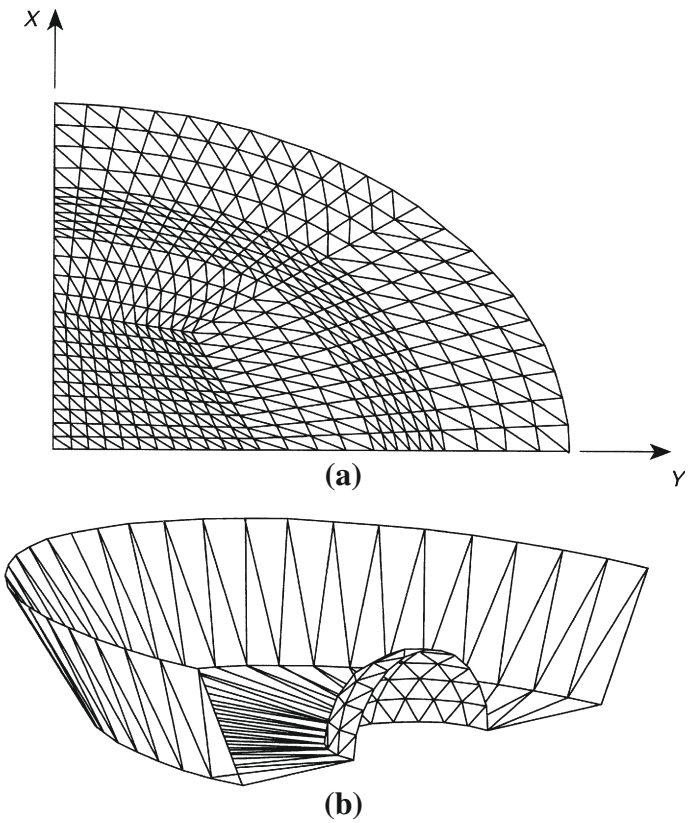

FIGURE 5.8
Finite element simulation of the superplastic forming of a thin sheet component by air pressure application. This example considers the superplastic forming of a truncated ellipsoid with a spherical indent. The original flat blank was 150×100 mm. The truncated ellipsoid is 20 mm deep. The original thickness was 1 mm. The minimum final thickness was 0.53 mm; 69 time steps were used with a total of 285 Newton-Raphson iterations (complete equation solutions) [53]: (a) mesh of 856 elements for sheet idealization; (b) mesh for establishing die geometry; (c) deformed sheets at various times.

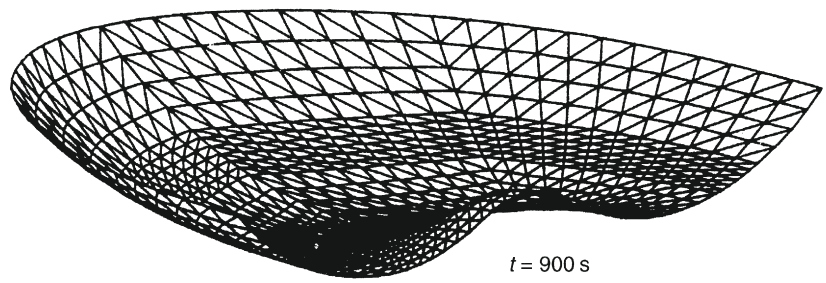

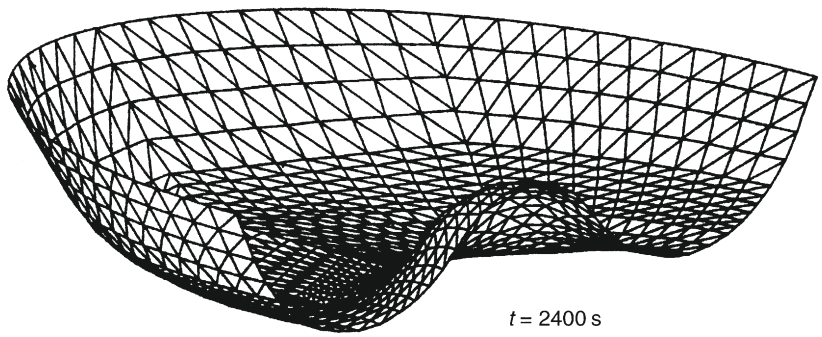

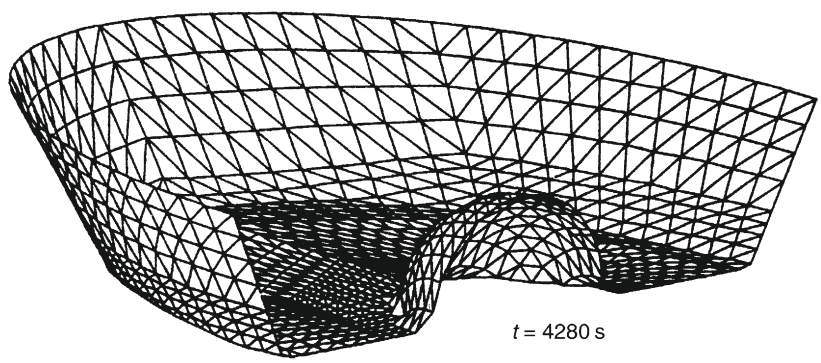

(c)

FIGURE 5.8
(*Continued*).

5.3 Viscoelastic flows

In this section we present a brief introduction to viscoelastic flow equations and their finite element solution using the CBS scheme. A good example of viscoelastic fluid is a polymeric liquid. Because of the memory (or spring-back) effect such fluids behave like an elastic material. A viscoelastic fluid can be represented by a number

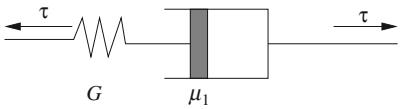

FIGURE 5.9
Physical representation of Maxwell model using spring and dashpot.

of springs and dashpots connected appropriately. In such a system, springs represent elastic effect and dashpots represent viscous behavior. One such system in series is shown in Fig. 5.9. Assuming $\dot{\gamma}$ to be the strain rate of the series, the stress τ will satisfy the following relation:

$$\tau + \lambda \frac{\delta \tau}{\delta t} = \mu_1 \dot{\gamma} \tag{5.12}$$

where μ_1 is the viscosity and λ is the relaxation time $= \mu_1/G$, with G being the spring constant. The above equation is widely known as the Maxwell equation. The above equation can easily be generalized to three dimensions. However, Eq. (5.12) does not obey the "objectivity rule." The generalization of the Maxwell model to satisfy the objectivity rule is carried out by replacing the time derivative with the upper convected time derivative, i.e., replace Eq. (5.12) with

$$\tau + \lambda \left(\frac{\partial \tau}{\partial t} + u \frac{\partial \tau}{\partial x} \right) = \mu_1 \dot{\gamma} \tag{5.13}$$

In multidimensions the constitutive equation becomes

$$\tau_{ij} + \lambda \left(\frac{\partial \tau_{ij}}{\partial t} + u_k \frac{\partial \tau_{ij}}{\partial x_k} \right) = \mu_1 \left(\frac{\partial u_i}{\partial x_j} + \frac{\partial u_j}{\partial x_i} \right) \tag{5.14}$$

In viscoelastic flows, τ_{ij} calculated from constitutive equations generally replace the deviatoric stress in the momentum equation. Another popular model used by many researchers is the Oldroyd-B model. Here, stresses generated by a Newtonian solvent and polymer solution are combined. In addition to the spring and dashpot shown in Fig. 5.9, a Newtonian dashpot is connected to the system in parallel when deriving the Oldroyd-B model as shown in Fig. 5.10. If we assume τ_v to be the stress developed

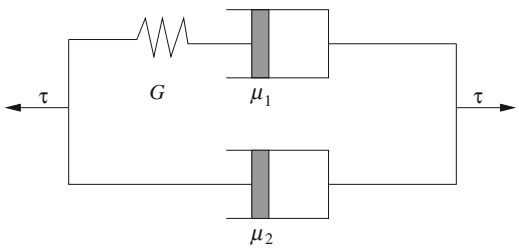

FIGURE 5.10
Physical representation of Oldroyd-B model using spring and dashpots.

by the polymer solution and τ_n is the stress developed by the Newtonian solvent, the Oldroyd-B model may be written as

$$\tau_v + \lambda \frac{\delta \tau_v}{\delta t} = \mu_1 \left(\frac{\partial u_i}{\partial x_j} + \frac{\partial u_j}{\partial x_i} \right) + \tau_n + \lambda \frac{\delta \tau_n}{\delta t} \tag{5.15}$$

With $\tau_n = \mu_2 \dot{\gamma}$ we get

$$\tau_v + \lambda \frac{\delta \tau_v}{\delta t} = \mu_1 \left(\frac{\partial u_i}{\partial x_j} + \frac{\partial u_j}{\partial x_i} \right) + \mu_2 \left(\frac{\partial u_i}{\partial x_j} + \frac{\partial u_j}{\partial x_i} \right) + \mu_2 \lambda \frac{\delta \dot{\gamma}}{\delta t} \tag{5.16}$$

where μ_2 is the viscosity of the Newtonian solvent. Rearranging and substituting $\mu = \mu_1 + \mu_2$, we get

$$\tau_v + \lambda \frac{\delta \tau_v}{\delta t} = \mu \left[\left(\frac{\partial u_i}{\partial x_j} + \frac{\partial u_j}{\partial x_i} \right) + \lambda_R \frac{\delta \dot{\gamma}}{\delta t} \right] \tag{5.17}$$

In the above equation λ_R is the retardation time given as $\mu_2 \lambda / \mu$. In order to satisfy the objectivity rule the $\delta / \delta t$ terms need to be replaced with the upper convected derivatives as in Eq. (5.14). In the following subsection we present a generalized form of the Maxwell and Oldroyd-B models together with the equilibrium equations to solve viscoelastic flows. Further details on constitutive modeling of viscoelastic flows may be found in Refs. [63,87].

5.3.1 Governing equations

The governing equations of viscoelastic flow can be written as follows:
Continuity equation

$$\frac{\partial \rho}{\partial t} + \frac{\partial}{\partial x_i}(U_i) = 0 \tag{5.18}$$

Momentum equation

$$\frac{\partial U_i}{\partial t} + \frac{\partial}{\partial x_j}(u_j U_i) = -\frac{\partial p}{\partial x_i} + \frac{\partial \tau_{ij}^n}{\partial x_j} + \frac{\partial \tau_{ij}^v}{\partial x_j} \tag{5.19}$$

where $U_i = \rho u_i$, ρ is the density, u_i are the velocity components, p is the pressure, and x_i are the coordinate directions. The superscript n in the above momentum equation indicates the Newtonian stress and superscript v indicates the non-Newtonian viscoelastic part of the stress. The Newtonian part of the stress relation can be written as

$$\tau_{ij}^n = \mu_2 \left(\frac{\partial u_i}{\partial x_j} + \frac{\partial u_j}{\partial x_i} \right) \tag{5.20}$$

In the above equation μ_2 is the Newtonian dynamic viscosity. The non-Newtonian extra stress tensor is expressed in conservation form as

$$\tau_{ij}^v + \lambda \left(\frac{\partial \tau_{ij}^v}{\partial t} + \frac{\partial}{\partial x_k} \left(u_k \tau_{ij}^v \right) \right) = \lambda \left(\tau_{ik}^v \frac{\partial u_j}{\partial x_k} + \tau_{jk}^v \frac{\partial u_i}{\partial x_k} \right) + \mu_1 \left(\frac{\partial u_i}{\partial x_j} + \frac{\partial u_j}{\partial x_i} \right) \tag{5.21}$$

In the above equation, μ_1 is the viscosity of viscoelastic contribution and λ is the relaxation time. It should be noted that the transient density term in the continuity equation can be replaced by the following pseudo pressure term for incompressible flows as discussed in Chapter 3:

$$\frac{\partial \rho}{\partial t} = \frac{1}{\beta^2}\frac{\partial p}{\partial t} \tag{5.22}$$

where β is an artificial compressibility parameter (or artificial wave speed). The problem is completed by specifying appropriate initial and boundary conditions for u_i, p, and extra stresses. The nondimensional form of the governing equations can be obtained by employing the following scales:

$$\begin{gathered} u_i^* = \frac{u_i}{u_\infty}, \quad \rho^* = \frac{\rho}{\rho_\infty}, \quad x_i^* = \frac{x_i}{L} \\ t^* = \frac{t u_\infty}{L}, \quad p^* = \frac{pL}{\mu u_\infty}, \quad \tau_{ij}^{2*} = \frac{\tau_{ij}^v L}{\mu u_\infty} \end{gathered} \tag{5.23}$$

where u_∞ is the free stream velocity, ρ_∞ is the free stream density, and L is any characteristic length. The nondimensional forms of the equations are:

Continuity equation

$$\frac{\partial \rho^*}{\partial t^*} + \frac{\partial U_i^*}{\partial x_i^*} = 0 \tag{5.24}$$

Momentum equation

$$\frac{\partial U_i^*}{\partial t^*} + \frac{\partial}{\partial x_j^*}\left(u_j^* U_i^*\right) = -\frac{1}{Re}\frac{\partial p^*}{\partial x_i^*} + \frac{1}{Re}\left(\alpha\frac{\partial \tau_{ij}^{n*}}{\partial x_j^*} + \frac{\partial \tau_{ij}^{v*}}{\partial x_j^*}\right) \tag{5.25}$$

Constitutive equation

$$\begin{aligned} \tau_{ij}^{v*} + De\left(\frac{\partial \tau_{ij}^{v*}}{\partial t^*} + \frac{\partial}{\partial x_k{}^*}(u_k{}^* \tau_{ij}^{v*})\right) &= De\left(\tau_{ik}^{v*}\frac{\partial u_j{}^*}{\partial x_k{}^*} + \tau_{jk}^{v*}\frac{\partial u_i{}^*}{\partial x_k{}^*}\right) \\ &\quad + (1-\alpha)\left(\frac{\partial u_i{}^*}{\partial x_j{}^*} + \frac{\partial u_j{}^*}{\partial x_i{}^*}\right) \end{aligned} \tag{5.26}$$

In the above nondimensional equations

$$\tau_{ij}^{n*} = \left(\frac{\partial u_i^*}{\partial x_j^*} + \frac{\partial u_j^*}{\partial x_i^*}\right) \tag{5.27}$$

Re is the Reynolds number and De is the Deborah number defined as

$$Re = \frac{\rho_\infty u_\infty L}{\mu}, \quad De = \frac{\lambda u_\infty}{L} \tag{5.28}$$

Here $\alpha = \mu_2/\mu$. With $\alpha = 0$ we recover the upper-convected Maxwell (UCM) model and $\alpha \neq 0$ gives the Oldroyd-B model. For incompressible viscoelastic flows the density term in Eq. (5.24) disappears.

The equations discussed above along with appropriate boundary conditions will form the governing equation system for solving viscoelastic flow problems. The solution procedure adopted here is the CBS scheme explained in Chapter 3 [77,80,81]. The basic three steps are the same as for Newtonian incompressible flows. However, an additional fourth step is necessary to get solutions to the constitutive equations. The simple explicit characteristic-Galerkin approach is adopted here to solve the constitutive equations. Additional dissipation is necessary at higher Deboroh numbers to smooth overshoots in the solution if a fully explicit scheme is used. The artificial dissipation methods are discussed in Chapter 7. The method used in the examples of the next section is a second-order method with a pressure switch [77].

Example 5.4. Viscoelastic flow past a circular cylinder

The problem definition is shown in Fig. 5.11. A circular cylinder of radius R is placed between two solid walls of a channel. The distances to inlet and exit from the center of the cylinder are $12R$ and $16R$ respectively. The top and bottom walls are assumed to be at a distance of $2R$ from the center of the cylinder. The Deborah number De is defined based on the radius R of the cylinder as

$$De = \frac{\lambda u_\infty}{R} \tag{5.29}$$

The following nondimensional forms of boundary conditions are employed in the flow calculations [88]. At inlet and exit $u_2 = 0$,

$$u_1 = 1.5(1 - \tfrac{1}{4}x_2^2) \tag{5.30a}$$

$$\tau_{11}^v = \tfrac{9}{8}(De)x_2^2 \tag{5.30b}$$

$$\tau_{12}^v = -\tfrac{3}{4}x_2 \tag{5.30c}$$

and $\tau_{22}^v = 0$. On solid walls (both channel walls and cylinder surface), no-slip conditions ($u_1 = 0$ and $u_2 = 0$) are assumed. The stress boundary conditions on the solid channel walls are given as

$$\tau_{11}^v = 2\alpha De\left(\frac{\partial u_1}{\partial x_2}\right)^2 \tag{5.31a}$$

$$\tau_{12}^v = \alpha\frac{\partial u_1}{\partial x_2} \tag{5.31b}$$

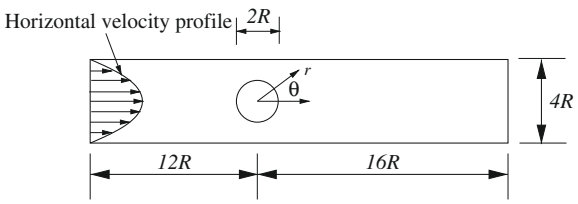

FIGURE 5.11
Viscoelastic flow past a circular cylinder. Geometry and boundary conditions.

and $\tau_{22} = 0$. On the cylinder wall the stress boundary conditions are similar to those above but in cylindrical coordinates. Thus the stress boundary conditions on the cylinder surface are

$$\tau_{\theta\theta} = 2\alpha De \left(\frac{\partial u_\theta}{\partial r}\right)^2 \tag{5.32a}$$

$$\tau_{r\theta} = \alpha \frac{\partial u_\theta}{\partial r} \tag{5.32b}$$

and $\tau_{rr} = 0$. Note that a transformation of quantities from cylindrical coordinate to Cartesian coordinates is essential in order to apply boundary conditions on the cylinder surface. To compare the present results with those available in the literature [88,89], the Reynolds number is assumed to be equal to zero and $\alpha = 0.41$ for this problem. The axial drag force on the cylinder per unit length is calculated in nondimensional form as

$$F_x = \int_0^{2\pi} \left[\left(-p + \tau_{11}^n + \tau_{11}^v\right)\cos\theta + \left(\tau_{12}^n + \tau_{12}^v\right)\sin\theta\right] R\mathrm{d}\theta \tag{5.33}$$

The details for meshes are given in Table 5.2 (for a full cylinder).

Figure 5.12 shows Mesh4, which is used in all the calculations. Note that due to symmetry [88,89], only one half of the domain is used in the calculations. The closeup of the mesh in the vicinity of the cylinder is shown in Fig. 5.12b. As seen the mesh is very fine close to the cylinder surface.

Figure 5.13 shows the contours of velocity and pressure for Newtonian flow at $Re = 0$. These patterns are in excellent agreement with the results reported in the literature [90]. The drag force calculated for this Newtonian case on Mesh4 is compared with reported fine mesh results in Table 5.3.

Figure 5.14 gives the contours of nondimensional velocity components, pressure, and extra stress components for a Deborah number of 0.5. All variable distributions are generally smooth without exhibiting any appreciable oscillatory behavior. These images show the existence of a strong stress gradient on the cylinder surface and on the solid side wall in the vicinity of the cylinder, which is an indication of the converging-diverging effect between the cylinder and the wall.

Figure 5.15 shows the comparison of drag forces calculated by different authors. The difference in the drag force values of different methods is small up to a Deborah number value of 0.4. However at higher De differences do exist between the methods. The results of Sun et al. [89] and Liu et al. [92] are produced on structured meshes.

Table 5.2 Details of Unstructured Meshes Employed

Mesh	Nodes	Elements	Typical Element Size on the Cylinder Surface
Mesh1	3151	5980	0.1
Mesh2	5848	11,272	0.051
Mesh3	12,217	23,832	0.022
Mesh4	21,238	40,768	0.016

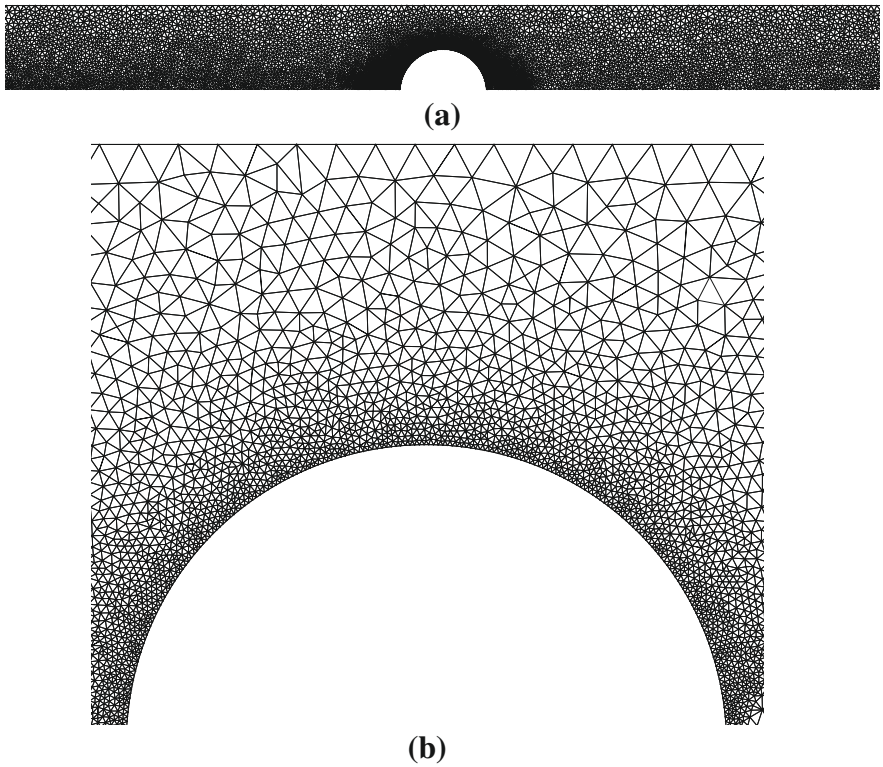

FIGURE 5.12
Viscoelastic flow past a circular cylinder. Unstructured mesh (nodes: 10,619; elements: 20,384): (a) mesh; (b) mesh in the vicinity of the cylinder.

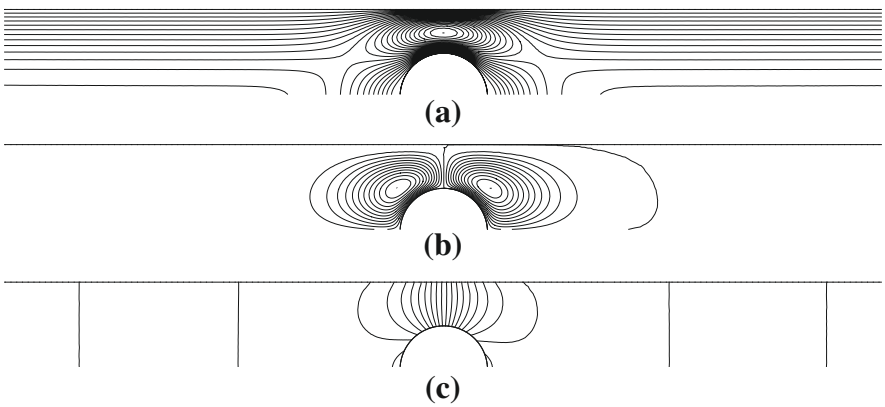

FIGURE 5.13
Stokes flow past a circular cylinder. $Re = 0$, $De = 0.0$. Contours of velocity components and pressure: (a) u_1 velocity contours, $u_{1_{\min}} = 0$, $u_{1_{\max}} = 2.94$; (b) u_2 velocity contours, $u_{2_{\min}} = -0.895$, $u_{2_{\max}} = 0.893$; (c) pressure contours, $p_{\min} = -29.28$, $p_{\max} = 36.04$.

Table 5.3 Comparison of Drag Force for the Newtonian Case

[88]	[91]	[89]	[90]	[92]	CBS
131.74	132.29	132.28	132.34	132.34	132.39

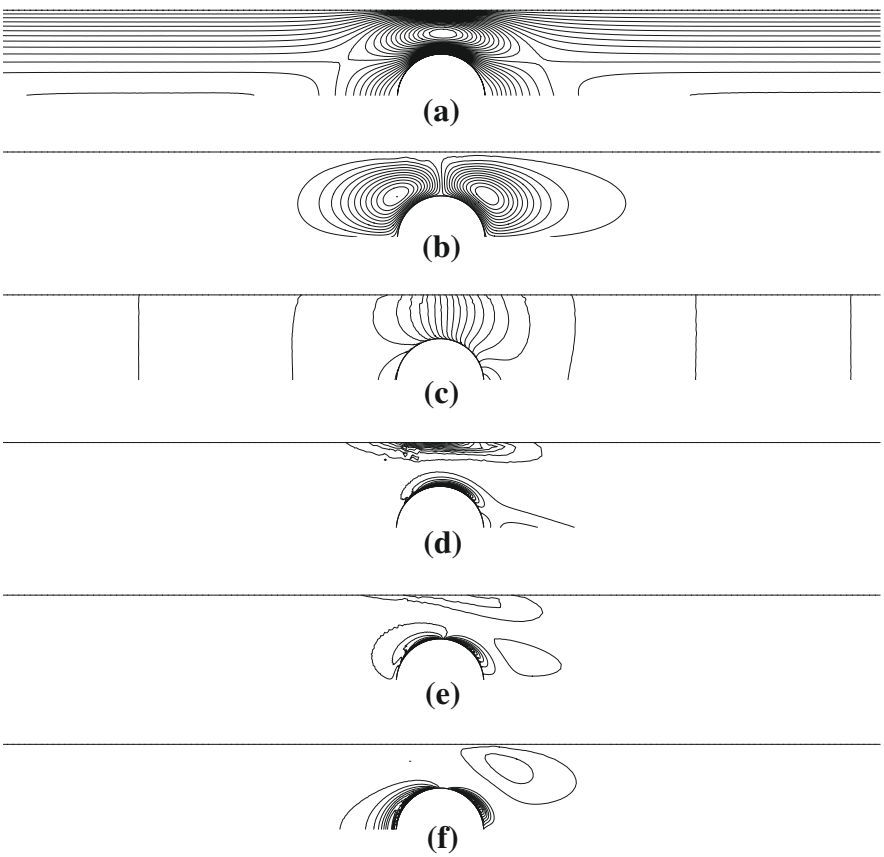

FIGURE 5.14

Viscoelastic flow past a circular cylinder. $Re = 0$, $De = 0.5$. Contours of velocity, pressure, and elastic stresses: (a) u_1 velocity contours, $u_{1_{\min}} = 0$, $u_{1_{\max}} = 2.99$; (b) u_2 velocity contours, $u_{2_{\min}} = -0.929$, $u_{2_{\max}} = 0.884$; (c) pressure contours, $p_{\min} = -28.35$, $p_{\max} = 34.97$; (d) τ^v_{11} contours, $\tau^v_{11_{\min}} = -0.979$, $\tau^v_{11_{\max}} = 76.45$; (e) τ^v_{12} contours, $\tau^v_{12_{\min}} = -18.59$, $\tau^v_{12_{\max}} = 22.92$; (f) τ^v_{22} contours, $\tau^v_{22_{min}} = -0.463$, $\tau^v_{22_{\max}} = 16.82$.

Understandably they are more accurate compared to other reported results. It is also noticed that the extrapolated drag force for a zero mesh size given by Dou and Phan-Thian [88] matches excellently with the results of Liu et al. [92] and Sun et al.

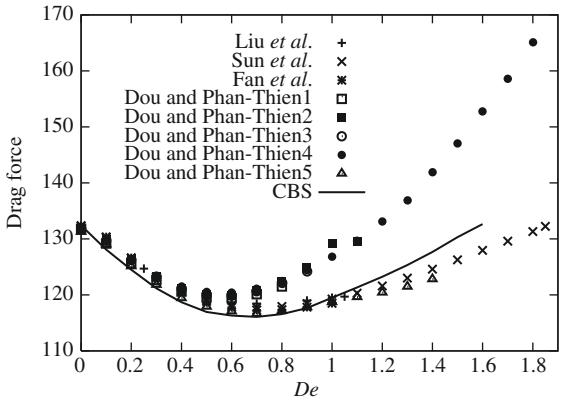

FIGURE 5.15

Viscoelastic flow past a circular cylinder. Comparison of drag force distribution with other available numerical data. Dou and Phan-Thian1 = Plain Oldroyd-B formulation without stress splitting; Dou and Phan-Thian2 = EVSS; Dou and Phan-Thian3 = DEVSS-ω; Dou and Phan-Thian4 = DAVSS-ω; Dou and Phan-Thian5 = Extrapolated results for zero mesh size.

[89] and to some extent agrees with the results of CBS. It should be noted the present CBS results are produced on a high-resolution unstructured mesh with a typical minimum size on the cylinder surface of around 0.01. However, the minimum size used by Dou and Phan-Thian [88] is 0.0402.

5.4 Direct displacement approach to transient metal forming

Explicit dynamic codes using quadrilateral or hexahedral elements have achieved considerable success in modeling short-duration impact phenomena with plastic deformation. The prototypes of finite element codes of this type are DYNA2d and DYNA3d, developed at Lawrence Livermore National Laboratory [93,94]. For problems of relatively slow metal forming, such codes present some difficulties as in general the time step is governed by the elastic compressibility of the metal and a vast number of time steps would be necessary to cover a realistic metal forming problem. Nevertheless much use has been made of such codes in slow metal forming processes by the simple expedient of increasing the density of the material by many orders of magnitude. This is one of the drawbacks of using such codes whose description rightly belongs to the matter discussed in Ref. [1]. However, a further drawback is the lack of triangular or tetrahedral elements of a linear kind which could compete with linear quadrilaterals or hexahedra currently used and permit an easier introduction of adaptive refinement. It is well known that linear triangles or tetrahedra in a pure displacement (velocity) formulation will lock for incompressible

or nearly incompressible materials. However, we have already found that the CBS algorithm will avoid such locking even if the same (linear) interpolation is used for both velocities and pressure [95].

It is therefore possible to proceed in each step by solving a simple Stokes problem to evaluate the Lagrangian velocity increment. We have described the use of such velocity formulation in the previous chapter. The update of the displacement allows new stresses to be evaluated by an appropriate plasticity law and the method can be used without difficulty as shown by Zienkiewicz et al. [95].

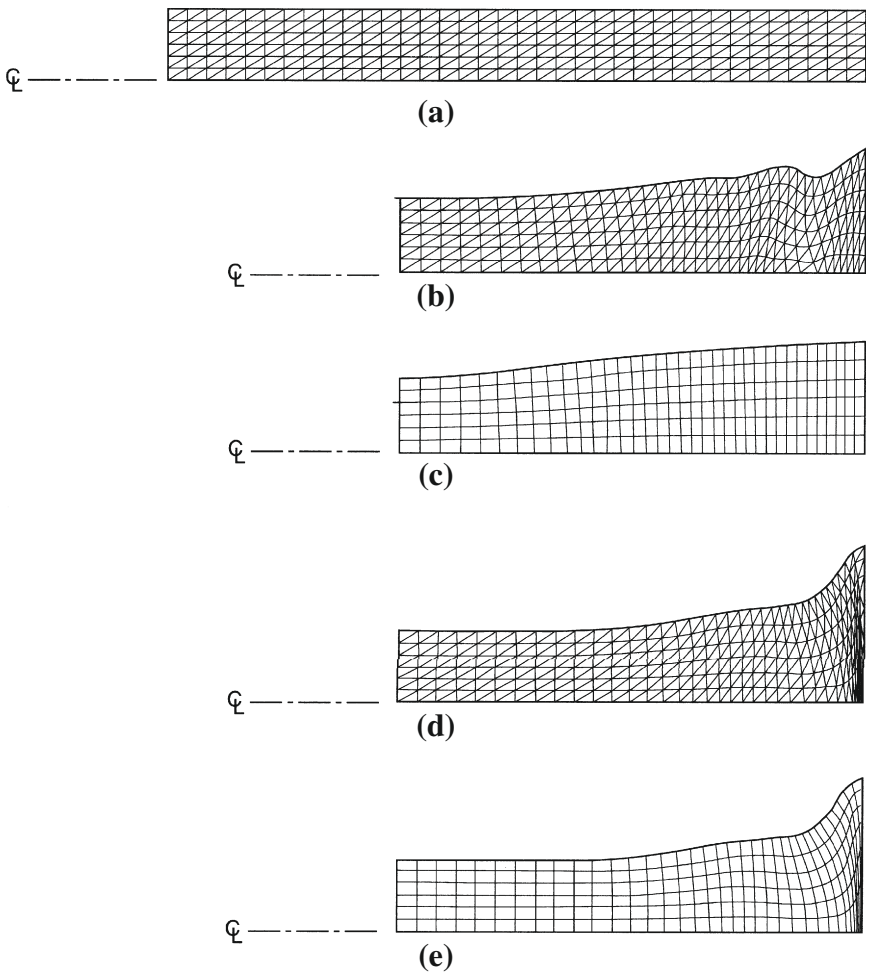

FIGURE 5.16
Axisymmetric solutions to the bar impact problem: (a) initial shape; (b) linear triangles—displacement algorithm; (c) bilinear quadrilaterals—displacement algorithm; (d) linear triangles—CBS algorithm; (e) bilinear quadrilaterals—CBS algorithm.

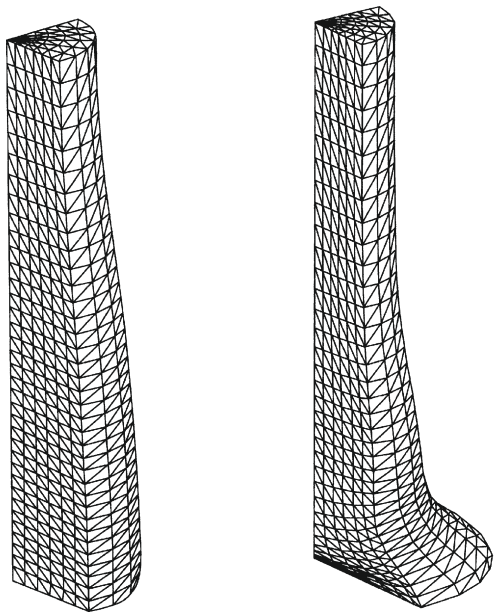

FIGURE 5.17
Three-dimensional solution: (a) tetrahedral elements—standard displacement algorithm; (b) tetrahedral elements—CBS algorithm.

Example 5.5. Impact of a circular bar

In Fig. 5.16, we show a comparison between various methods of solving the impact of a circular bar made of an elastoplastic metal using an axisymmetric formulation. In this figure we show the results of a linear triangle displacement (Fig. 5.16b) form with a single integrating point for each element and a similar study again using displacement linear quadrilaterals (Fig. 5.16c) also with a single integration point. This figure also shows the same triangles and quadrilaterals solved using the CBS algorithm and now giving very accurate final results (Fig. 5.16d and e).

In Fig. 5.17 we show similar results obtained with a full three-dimensional analysis. Similar methods for this problem have been presented by Bonet and Burton [96].

5.5 Concluding remarks

The range of examples for which an incompressible formulation applies is very large as we have shown in this chapter. Indeed many other examples could have been included but for lack of space we proceed directly to Chapter 6 where the incompressible formulation is used for problems in which free surface or buoyancy occurs, with gravity forces being the most important factor.

References

[1] O.C. Zienkiewicz, R.L. Taylor, D.D. Fox, The Finite Element Method for Solids and Structural Mechanics, seventh ed., Elsevier, Oxford, 2013.
[2] K. Palit, R.T. Fenner, Finite element analysis of two dimensional slow non-Newtonian flows, AIChE J. 18 (1972) 1163–1169.
[3] B. Atkinson, C.C.M. Card, B.M. Irons, Application of the finite element method to creeping flow problems, Trans. Inst. Chem. Eng. 48 (1970) 276–284.
[4] O.C. Zienkiewicz, P.N. Godbole, A penalty function approach to problems of plastic flow of metals with large surface deformation, J. Strain Anal. 10 (1975) 180–183.
[5] G.C. Cornfield, R.H. Johnson, Theoretical prediction of plastic flow in hot rolling including the effect of various temperature distributions, J. Iron Steel Inst. 211 (1973) 567–573.
[6] C.H. Lee, S. Kobayashi, New solutions to rigid plastic deformation problems using a matrix method, Trans. ASME J. Eng. Ind. 95 (1973) 865–873.
[7] J.T. Oden, D.R. Bhandari, G. Yagewa, T.J. Chung, A new approach to the finite element formulation and solution of a class of problems in coupled thermoelastoviscoplasticity of solids, Nucl. Eng. Des. 24 (1973) 420.
[8] R.E. Nickell, R.I. Tanner, B. Caswell, The solution of viscous incompressible jet and free surface flows using finite elements, J. Fluid Mech. 65 (1974) 189–206.
[9] R.I. Tanner, R.E. Nickell, R.W. Bilger, Finite element method for the solution of some incompressible non-Newtonian fluids mechanics problems with free surface, Comput. Methods Appl. Mech. Eng. 6 (1975) 155–174.
[10] J.M. Alexander, J.W.H. Price, Finite element analysis of hot metal forming, in: Proceedings of 18th MTDR Conference, 1977, pp. 267–274.
[11] O.C. Zienkiewicz, P.C. Jain, E. Oñate, Flow of solids during forming and extrusion: some aspects of numerical solutions, Int. J. Solids Struct. 14 (1978) 15–38.
[12] P.R. Dawson, E.G. Thompson, Finite element analysis of steady state elastoviscoplastic flow by the initial stress rate method, Int. J. Numer. Methods Eng. 12 (1978) 47–57.
[13] O.C. Zienkiewicz, E. Oñate, J.C. Heinrich, Plastic flow in metal forming, in: Proceedings of the Winter Annual Meeting of ASME, San Francisco, December 1978, pp. 107–120.
[14] N. Rebelo, S. Kobayashi, A coupled analysis of viscoplastic deformation and heat transfer: I. Theoretical consideration, Int. J. Mech. Sci. 22 (1980) 699–705.
[15] O.C. Zienkiewicz, E. Oñate, J.C. Heinrich, A general formulation for coupled thermal flow of metals using finite elements, Int. J. Numer. Methods Eng. 17 (1980) 1497–1514.
[16] Y. Shimizaki, E.G. Thompson, Elasto-visco-plastic flow with special attention to boundary conditions, Int. J. Numer. Meth. Eng. 17 (1981) 97–112.
[17] S. Nakazawa, J.F. Pittman, O.C. Zienkiewicz, Numerical solution of flow and heat transfer in polymer melts, in: R.H. Gallagher et al. (Eds.), Finite Elements in Fluids, vol. 4, John Wiley & Sons, Chichester, 1982, pp. 251–283 (Chapter 13).

[18] S. Nakazawa, J.F.T. Pittman, O.C. Zienkiewicz, A penalty finite element method for thermally coupled non-Newtonian flow with particular reference to balancing dissipation and the treatment of history dependent flows, in: International Symposium of Refined Modelling of Flows, Ecole Nationale des Ponts et Chaussees, Paris, September 1982, pp. 7–10.
[19] S.I. Oh, G.D. Lahoti, A.T. Altan, Application of finite element method to industrial metal forming processes, in: Proceedings of Conference on Industrial Forming Processes, Pineridge Press, Swansea, 1982, pp. 146–153.
[20] J.F.T. Pittman, O.C. Zienkiewicz, R.D. Wood, J.M. Alexander (Eds.), Numerical Analysis of Forming Processes, John Wiley & Sons, Chichester, 1984.
[21] O.C. Zienkiewicz, Flow formulation for numerical solutions of forming problems, in: J.F.T. Pittman et al. (Eds.), Numerical Analysis of Forming Processes, John Wiley & Sons, Chichester, 1984, pp. 1–44 (Chapter 1).
[22] S. Kobayashi, Thermoviscoplastic analysis of metal forming problems by the finite element method, in: J.F.T. Pittman et al. (Eds.), Numerical Analysis of Forming Processes, John Wiley & Sons, Chichester, 1984, pp. 45–70 (Chapter 2).
[23] J.L. Chenot, F. Bay, L. Fourment, Finite element simulation of metal powder forming, Int. J. Numer. Meth. Eng. 30 (1990) 1649–1674.
[24] P.A. Balaji, T. Sundararajan, G.K. Lal, Viscoplastic deformation analysis and extrusion die design by FEM, J. Appl. Mech. Trans. ASME 58 (1991) 644–650.
[25] K.H. Raj, J.L. Chenot, L. Fourment, Finite element modelling of hot metal forming, Indian J. Eng. Mat. Sci. 3 (1996) 234–238.
[26] J.L. Chenot, Recent contributions to the finite element modelling of metal forming processes, J. Mater. Process. Technol. 34 (1992) 9–18.
[27] J. Bonet, P. Bhargava, R.D. Wood, The incremental flow formulation for the finite element analysis of 3-dimensional superplastic forming processes, J. Mater. Process. Technol. 45 (1994) 243–248.
[28] R.D. Wood, J. Bonet, A review of the numerical analysis of super-plastic forming, J. Mater. Process. Technol. 60 (1996) 45–53.
[29] J.L. Chenot, Y. Chastel, Mechanical, thermal and physical coupling methods in FE analysis of metal forming processes, J. Mater. Process. Technol. 60 (1996) 11–18.
[30] D. Brokken, W.A.M. Brekelmans, F.P.T. Baaijens, Numerical modelling of the metal blanking process, J. Mater. Process. Technol. 83 (1–3) (1998) 192–199.
[31] J. Rojek, E. Oñate, E. Postek, Application of explicit FE codes to simulation of sheet and bulk metal forming processes, J. Mater. Process. Technol. 80 (1998) 620–627.
[32] S.W. Hsiao, N. Kikuchi, Numerical analysis and optimal design of composite thermoforming process, Comput. Methods Appl. Mech. Eng. 177 (1–2) (1999) 1–34.
[33] J. Bonet, A.J. Gil, Finite element modelling of thin metal sheet forming, in: G. Giuliano (Ed.), Superplastic Forming of Advanced Metallic Materials: Methods and Applications, Woodhead Publishing in Materials, 2011, pp. 136–153.

[34] J.-L. Chenot, R.D. Wood, O.C. Zienkiewic (Eds.), Numerical Methods in Industrial Forming Processes: NUMIFORM 92, Valbonne, France, 14–19, A.A. Balkema, Rotterdam, September 1992.

[35] J. Húetink, F.P.T. Baaijens (Eds.), Simulation of Materials Processing: Theory, Methods and Applications: NUMIFORM 98, Enschede, Netherlands, A.A. Balkema, Rotterdam, 22–25 june 1998.

[36] S. Ghosh, J.M. Castro, J.K. Lee (Eds.), Materials Processing and Design: Theory, Methods and Applications, NUMIFORM 2004, American Institute of Physics, 2004.

[37] Jose M.A. Cesar de Sa, Abel D. Santos (Eds.), Materials Processing and Design: Modeling, Simulation and Applications, NUMIFORM 2007: Proceedings of the 9th International Conference on Numerical Methods in Industrial Forming Processes. AIP Conference Proceedings 908, 2007.

[38] F. Barlat, Y.H. Moon, M.G. Lee (Eds.), NUMIFORM 2010: Proceedings of the 10th International Conference on Numerical Methods in Industrial Forming Processes Dedicated to Professor O.C. Zienkiewicz (1921–2009), AIP Conference Proceedings, vol. 1252, 2010.

[39] W. Johnson, P.B. Mellor, Engineering Plasticity, Van Nostrand-Reinhold, London, 1973.

[40] O.C. Zienkiewicz, Y.C. Liu, G.C. Huang, Error estimates and convergence rates for various incompressible elements, Int. J. Numer. Methods Eng. 28 (1989) 2191–2202.

[41] G.C. Huang, Error estimates and adaptive remeshing in finite element analysis of forming processes, Ph.D Thesis, Department of Civil Engineering, University of Wales, Swansea, 1989.

[42] G.C. Huang, Y.C. Liu, O.C. Zienkiewicz, Error control, mesh updating schemes and automatic adaptive remeshing for finite element analysis of unsteady extrusion processes, in: J.L. Chenot, E. Oñate (Eds.), Modelling of Metal Forming Processes, Kluwer Academic, Dordrecht, 1988, pp. 75–83.

[43] O.C. Zienkiewicz, Y.C. Liu, G.C. Huang, An error estimate and adaptive refinement method for extrusion and other forming problems, Int. J. Numer. Methods Eng. 25 (1988) 23–42.

[44] O.C. Zienkiewicz, Y.C. Liu, J.Z. Zhu, S. Toyoshima, Flow formulation for numerical solution of forming processes. II—Some new directions, in: K. Mattiasson, A. Samuelsson, R.D. Wood, O.C. Zienkiewicz (Eds.), Proceedings of 2nd International Conference on Numerical Methods in Industrial Forming Processes, NUMIFORM 86, A.A. Balkema, Rotterdam, 1986.

[45] T. Belytschko, D.P. Flanagan, J.M. Kennedy, Finite element methods with user controlled mesh for fluid structure interaction, Comput. Methods Appl. Mech. Eng. 33 (1982) 669–688.

[46] J. Donea, S. Giuliani, H. Laval, L. Quartapelle, Finite element solution of unsteady Navier-Stokes equations by a fractional step method, Comput. Methods Appl. Mech. Eng. 33 (1982) 53–73.

[47] P.J.G. Schreurs, F.E. Veldpaus, W.A.M. Brakalmans, An Eulerian and Lagrangian finite element model for the simulation of geometrical non-linear hyper-elastic and elasto-plastic deformation processes, in: Proceedings of Conference on Industrial Forming Processes, Pineridge Press, Swansea, 1983, pp. 491–500.
[48] J. Donea, Arbitrary Lagrangian-Eulerian finite element methods, in: T. Belytschko, T.J.R. Hughes (Eds.), Computation Methods for Transient Analysis, Elsevier, Amsterdam, 1983, pp. 474–516 (Chapter 10).
[49] J. van der Lugt, J. Huetnik, Thermo-mechanically coupled finite element analysis in metal forming processes, Comput. Methods. Appl. Mech. Eng. 54 (1986) 145–160.
[50] E. Oñate, O.C. Zienkiewicz, A viscous sheet formulation for the analysis of thin sheet metal forming, Int. J. Mech. Sci. 25 (1983) 305–335.
[51] N.M. Wang, B. Budiansky, Analysis of sheet metal stamping by a finite element method, J. Appl. Mech. ASME 45 (1976) 73.
[52] A.S. Wifi, An incremented complete solution of the stretch forming and deep drawing of a circular blank using a hemispherical punch, Int. J. Mech. Sci. 18 (1976) 23–31.
[53] J. Bonet, R.D. Wood, O.C. Zienkiewicz, Time stepping schemes for the numerical analysis of superplastic forming of thin sheets, in: J.L. Chenot, E. Oñate (Eds.), Modelling of Metal Forming Processes, Kluwer Academic, Dordrecht, 1988, pp. 179–186.
[54] E. Massoni, M. Bellet, J.L. Chenot, Thin sheet forming numerical analysis with membrane approach, in: J.L. Chenot, E. Oñate (Eds.), Modelling of Metal Forming Processes, Kluwer Academic, Dordrecht, 1988.
[55] J. Bonet, R.D. Wood, O.C. Zienkiewicz, Finite element modelling of the superplastic forming of a thin sheet, in: C.H. Hamilton, N.E. Paton (Eds.), Proceedings Conference on Superquality and Superplastic Forming, The Minerals, Metals and Materials Society, USA, 1988.
[56] R.D. Wood, J. Bonet, A.H.S. Wargedipura, Simulation of the superplastic forming of thin sheet components using the finite element method, in: Proceedings of NUMIFORM 89, A.A. Balkema, Rotterdam, 1989, pp. 85–94.
[57] E. Oñate, C.A. Desaracibar, Finite element analysis of sheet metal forming problems using a selective bending membrane formulation, Int. J. Numer. Meth. Eng. 30 (1990) 1577–1593.
[58] W. Sosnowski, E. Oñate, C.A. Desaracibar, Comparative study of sheet metal forming processes by numerical modelling and experiment, J. Mater. Process. Technol. 34 (1992) 109–116.
[59] J. Bonet, R.D. Wood, Incremental flow procedures for the finite element analysis of thin sheet superplastic forming processes, J. Mater. Process. Technol. 42 (1994) 147–165.
[60] W. Sosnowski, M. Kleiber, A study on the influence of friction evolution on thickness changes in sheet metal forming, J. Mat. Proc. Tech. 60 (1996) 469–474.

[61] M. Kawka, T. Kakita, A. Makinouchi, Simulation of multi-step sheet metal forming processes by a static explicit FEM code, J. Mat. Proc. Tech. 80 (1998) 54–59.
[62] S.K. Esche, G.K. Kinzel, J.K. Lee, An axisymmetric membrane element with bending stiffness for static implicit sheet metal forming simulation, J. Appl. Mech. ASME 66 (1999) 153–164.
[63] M.J. Crochet, R. Keunings, Finite element analysis of die swell of highly elastic fluid, J. Non-Newtonian Fluid Mech. 10 (1982) 339–356.
[64] M.J. Crochet, A.R. Davies, K. Walters, Numerical simulation of non-Newtonian flow, Rheology Series, vol. 1, Elsevier, Amsterdam, 1984.
[65] R. Keunings, M.J. Crochet, Numerical simulation of the flow of a viscoelastic fluid through an abrupt contraction, J. Non-Newtonian Fluid Mech. 14 (1984) 279–299.
[66] S. Dupont, J.M. Marchal, M.J. Crochet, Finite element simulation of viscoelastic fluids of the integral type, J. Non-Newtonian Fluid Mech. 17 (1985) 157–183.
[67] J.M. Marchal, M.J. Crochet, A new mixed finite element for calculating visco elastic flow, J. Non-Newtonian Fluid Mech. 26 (1987) 77–114.
[68] M.J. Crochet, V. Legat, The consistent streamline upwind Petrov-Galerkin method for viscoelastic flow revisited, J. Non-Newtonian Fluid Mech. 42 (1992) 283–299.
[69] H.R. Tamaddonjahromi, D. Ding, M.F. Webster, P. Townsend, A Taylor-Galerkin finite element method for non-Newtonian flows, Int. J. Numer. Methods Eng. 34 (1992) 741–757.
[70] E.O.A. Carew, P. Townsend, M.F. Webster, A Taylor-Galerkin algorithm for viscoelastic flow, J. Non-Newtonian Fluid Mech. 50 (1993) 253–287.
[71] D. Ding, P. Townsend, M.F. Webster, Finite element simulation of an injection moulding process, Int. J. Num. Methods Heat Fluid Flow 7 (1997) 751–766.
[72] H. Matallah, P. Townsend, M.F. Webster, Recovery and stress-splitting schemes for viscoelastic flows, J. Non-Newtonian Fluid Mech. 75 (1998) 139–166.
[73] F.P.T. Baaijens, Mixed finite element methods for viscoelastic flow analysis: a review, J. Non-Newtonian Fluid Mech. 79 (2–3) (1998) 361–385.
[74] M.D. Smith, R.C. Armstrong, R.A. Brown, R. Sureshkumar, Finite element analysis of stability of two-dimensional viscoelastic flows to three-dimensional perturbations, J. Non-Newtonian Fluid Mech. 93 (2–3) (2000) 203–244.
[75] J. Petera, A new finite element scheme using the Lagrangian framework for simulation of viscoelastic fluid flows, J. Non-Newtonian Fluid Mech. 103 (2002) 1–43.
[76] A.G. Lee, E.S.G. Shaqfeh, B. Khomami, A study of viscoelastic free surface flows by the finite element method: Hele-Shaw and slot coating flows, J. Non-Newtonian Fluid Mech. 108 (1–3) (2002) 327–362.
[77] P. Nithiarasu, A fully explicit characteristic based split (CBS) scheme for viscoelastic flow calculations, Int. J. Numer. Methods Eng. 60 (5) (2004) 949–978.

[78] J.M. Kim, C. Kim, J.H. Kim, C. Chung, K.H. Ahn, S.J. Lee, High-resolution finite element simulation of 4:1 planar contraction flow of viscoelastic fluid, J. Non-Newtonian Fluid Mech. 129 (1) (2005) 23–37.
[79] P. Yue, C. Zhou, J.J. Feng, C.F. Ollivier-Gooch, H.H. Hu, Phase-field simulations of interfacial dynamics in viscoelastic fluids using finite elements with adaptive meshing, J. Comput. Phys. 219 (2006) 47–67.
[80] C.-B. Liu, P. Nithiarasu, The characteristic-based split (CBS) scheme for viscoelastic flow past a circular cylinder, Int. J. Numer. Methods Fluids 57 (2008) 157–176.
[81] C.-B. Liu, P. Nithiarasu, An artificial-dissipation-based fractional step scheme for upper-convected Maxwell (UCM) fluid flow past a circular cylinder, Int. J. Numer. Methods Fluids 57 (2008) 1171–1187.
[82] Z. Cai, C.R. Westphal, An adaptive mixed least-squares finite element method for viscoelastic fluids of Oldroyd type, J. Non-Newtonian Fluid Mech. 159 (1–3) (2009) 72–80.
[83] X. Li, H. Xianhong, W. Xuanping, Numerical modeling of viscoelastic flows using equal low-order finite elements, Comput. Methods Appl. Mech. Eng. 199 (9–12) (2010) 570–581.
[84] Y.-J. Lee, J. Xu, C.-S. Zhang, Stable finite element discretizations for viscoelastic flow models, in: R. Glowinski, J. Xu (Eds.), Special Volume: Numerical Methods for Non-Newtonian Fluids, Handbook of Numerical Analysis, vol. 16, Elsevier, 2011, pp. 371–432.
[85] W.R. Hwang, M.A. Walkley, O.G. Harlen, A fast and efficient iterative scheme for viscoelastic flow simulations with the DEVSS finite element method, J. Non-Newtonian Fluid Mech. 166 (7–8) (2011) 354–362.
[86] Y.J. Choi, M.A. Hulsen, H.E.H. Meijer, Simulation of the flow of a viscoelastic fluid around a stationary cylinder using an extended finite element method, Comput. Fluids 57 (2012) 183–194.
[87] N. Phan-Thien, Understanding Viscoelasticity. Basics of Rheology, Springer Verlag, Berlin, 2002.
[88] H.S. Dou, N. Phan-Thien, The flow of an Oldroyd-B fluid past a cylinder in a channel: adaptive viscosity vorticity (DAVSS-omega) formulation, J. Non-Newtonian Fluid Mech. 87 (1) (1999) 47–73.
[89] J. Sun, M.D. Smith, R.C. Armstrong, R.A. Brown, Finite element method for viscoelastic flows based on the discrete adaptive viscoelastic stress splitting and the discontinuous Galerkin method: DAVSS-G/DG, J. Non-Newtonian Fluid Mech. 86 (3) (1999) 281–307.
[90] E. Mitsoulis, Numerical simulation of confined flow of polyethylene melts around a cylinder in a planar channel, J. Non-Newtonian Fluid Mech. 76 (1–3) (1998) 327–350.
[91] Y.R. Fan, R.I. Tanner, N. Phan-Thien, Galerkin/least-square finite-element methods for steady viscoelastic flows, J. Non-Newtonian Fluid Mech. 84 (2–3) (1999) 233–256.

[92] A.W. Liu, D.E. Bornside, R.C. Armstrong, R.A. Brown, Viscoelastic flow of polymer solutions around a periodic, linear array of cylinders: comparisons of predictions for microstructure and flow fields, J. Non-Newtonian Fluid Mech. 77 (3) (1998) 153–190.

[93] G.L. Goudreau, J.O. Hallquist, Recent developments in large scale Lagrangian hydrocodes, Comput. Methods Appl. Mech. Eng. 33 (1982) 725–757.

[94] J.O. Hallquist, G.L. Goudreau, D.J. Benson, Sliding interfaces with contact-impact in large scale Lagrangian computations, Comput. Methods Appl. Mech. Eng. 51 (1985) 107–137.

[95] O.C. Zienkiewicz, J. Rojek, R.L. Taylor, M. Pastor, Triangles and tetrahedra in explicit dynamics codes for solids, Int. J. Numer. Methods Eng. 43 (1998) 565–583.

[96] J. Bonet, A.J. Burton, A simple average nodal pressure tetrahedral element for incompressible and nearly incompressible dynamic explicit applications, Commun. Numer. Methods Eng. 14 (1998) 437–449.